NASA TECHNICAL MEMORANDUM

NASA TM X-72709

NASA TM X-72709

FRACTURE ANALYSIS OF VARIOUS CRACKED CONFIGURATIONS IN SHEET AND PLATE MATERIALS

By J. C. Newman, Jr.
Langley Research Center
Hampton, VA 23665

TECHNICAL PAPER presented at the Symposium on Properties Related to Toughness, 1975, Annual ASTM Meeting, Montreal, Canada, June 23 - 27, 1975

NATIONAL AERONAUTICS AND SPACE ADMINISTRATION
LANGLEY RESEARCH CENTER, HAMPTON, VIRGINIA 23665

1. Report No.	2. Government Accession No.	3. Recipient's Catalog No.
NASA TMX-72709		

4. Title and Subtitle	5. Report Date
Fracture Analysis of Various Cracked Configurations In Sheet and Plate Materials	JULY 1975
	6. Performing Organization Code 2532
7. Author(s)	8. Performing Organization Report No.
James C. Newman, Jr.	
9. Performing Organization Name and Address	10. Work Unit No.
NASA Langley Research Center Hampton, VA 23665	505-02-31-01
	11. Contract or Grant No.
	13. Type of Report and Period Covered
12. Sponsoring Agency Name and Address	Technical Memorandum
National Aeronautics and Space Administration Washington, D.C. 20546	14. Sponsoring Agency Code

15. Supplementary Notes

Paper presented at the ASTM Symposium on Properties Related to Toughness, Montreal, Canada, June 23 - 27, 1975.

16. Abstract

A two-parameter fracture criterion has been derived which relates the linear-elastic stress-intensity factor at failure, the elastic nominal failure stress, and two material parameters. The fracture criterion was used previously to analyze fracture data for surface- and through-cracked sheet and plate specimens under tensile loading. In the present paper the fracture criterion was applied to center-crack tension, compact, and notch-bend fracture specimens made of steel, titanium, or aluminum alloy materials tested at room temperature. The fracture data included a wide range of crack lengths, specimen widths, and thicknesses. The materials analyzed had a wide range of tensile properties. Failure stresses calculated using the criterion agreed well (±10 percent) with experimental failure stresses. The criterion was also found to correlate fracture data from different specimen types (such as center-crack tension and compact specimens), within ±10 percent for the same material, thickness, and test temperature.

17. Key Words (Suggested by Author(s)) (STAR category underlined)	18. Distribution Statement
Fracture Stress-Intensity Factor Structural Mechanics Materials (Metallic)	Unclassified - Unlimited

19. Security Classif. (of this report)	20. Security Classif. (of this page)	21. No. of Pages	22. Price*
Unclassified	Unclassified	33	$3.75

*Available from { The National Technical Information Service, Springfield, Virginia 22151
STIF/NASA Scientific and Technical Information Facility, P.O. Box 33, College Park, MD 20740

FRACTURE ANALYSIS OF VARIOUS CRACKED CONFIGURATIONS IN SHEET AND PLATE MATERIALS

J. C. Newman, Jr.

NASA Langley Research Center

Hampton, Virginia 23665, U.S.A.

ABSTRACT

A two-parameter fracture criterion has been derived which relates the linear-elastic stress-intensity factor at failure, the elastic nominal failure stress, and two material parameters. The fracture criterion was used previously to analyze fracture data for surface- and through-cracked sheet and plate specimens under tensile loading. In the present paper the fracture criterion was applied to center-crack tension, compact, and notch-bend fracture specimens made of steel, titanium, or aluminum alloy materials tested at room temperature. The fracture data included a wide range of crack lengths, specimen widths, and thicknesses. The materials analyzed had a wide range of tensile properties. Failure stresses calculated using the criterion agreed well ($\pm$10 percent) with experimental failure stresses. The criterion was also found to correlate fracture data from different specimen types (such as center-crack tension and compact specimens), within $\pm$10 percent for the same material, thickness, and test temperature.

KEY WORDS: Fracture, Fracture Mechanics, Stress Intensity Factor, Cracks, Materials.

L-9716

INTRODUCTION

The concepts of Linear-Elastic Fracture Mechanics have been very useful in correlating fracture data for cracked plates and structural components in which the crack-tip plastic deformations are constrained to small regions (plane-strain fracture [1]). However, for high-toughness sheet materials where large amounts of plastic deformation occur near the crack tip at fracture, the elastic stress-intensity factor at failure (K_{Ie}) varies with planar dimensions, such as crack length and specimen width. (See [2]-[5].) To account for the variation in K_{Ie} with crack length and specimen width, the elastic-plastic stress-strain behavior near the crack tip must be considered.

Several equations for calculating the elastic-plastic stress-strain behavior at notches or cracks have been proposed. Among these are equations derived for notches by Hardrath and Ohman [6], and by Neuber [7]. For cracks, equations have been derived by Hutchinson [8] and by Rice and Rosengren [9]. The Hardrath-Ohman equation was later generalized for a cracked plate and was applied as a fracture criterion by Kuhn and Figge [10]. In a similar way, Newman [4, 5], using the Neuber relation and the elastic-stress distribution in the crack-tip region, derived a fracture criterion for a cracked plate which related the elastic stress-intensity factor at failure, the elastic nominal failure stress, and two material parameters. The two-parameter fracture criterion was used in [4] to analyze failure of surface- and through-cracked sheet and plate specimens under tensile loading. This criterion was rederived in a more general form in [5] and was used to analyze failure of compact and notch-bend sheet specimens.

In the present paper, the criterion was applied to center-crack tension, compact, and notch-bend sheet and plate specimens (Fig. 1) made of steel,

titanium, or aluminum alloy materials tested at room temperature. The fracture data included a wide range of crack lengths, specimen widths, and thicknesses. The materials analyzed had a wide range of tensile properties.

SYMBOLS

c	Initial length of crack defined in Figure 1, m
F	Boundary correction on the stress-intensity factor
K_F	Fracture toughness computed from Equation (2), $N/m^{3/2}$
K_I	Elastic stress-intensity factor, $N/m^{3/2}$
K_{Ie}	Elastic stress-intensity factor at failure, $N/m^{3/2}$
L	Major span length for notch-bend specimen, m
m	Fracture-toughness parameter
P	Applied load at failure, N
S	Gross failure stress, N/m^2
S_n	Elastic nominal stress (net section) at failure, N/m^2
S_u	Ultimate value of elastic nominal stress, N/m^2
t	Specimen thickness, m
W	Specimen width, m
γ	Function defined by Equation (6)
λ	Crack-length-to-specimen width ratio (defined in Fig. 1)
σ_u	Ultimate tensile strength, N/m^2
σ_{ys}	Uniaxial yield stress, N/m^2
ϕ	Ratio of K_{Ie} to K_F

TWO-PARAMETER FRACTURE CRITERION

The elastic-stress distribution near a crack tip in an elastic material which contains the stress-intensity factor, K_I, and the square-root singularity is well known [2]. The determination of K_I is the basis for Linear-Elastic

Fracture Mechanics. The stress-intensity factor is a function of the load, the configuration, and the size and location of the crack. In general, the elastic stress-intensity factor at failure for any cracked (Mode I) configuration can be expressed as

$$K_{Ie} = S_n \sqrt{\pi c}\ F \tag{1}$$

where S_n is the nominal failure stress (computed from the maximum load at failure) and c is the initial crack length. The boundary-correction factor, F, accounts for the influence of various boundaries on stress intensity. (Appendix A gives the equations for S_n and F for the center-crack, compact, and notch-bend specimens.) The use of the linear-elastic equation is restricted to conditions in which the plastic zone at the crack tip is very small compared to other dimensions of the body (brittle fracture [1]). Consequently, to analyze ductile materials, the elastic-plastic behavior of the stresses and strains near the crack tip must be considered.

A fracture criterion was derived [4, 5] that accounts for the elastic-plastic behavior of the material. This criterion is

$$K_F = \frac{K_{Ie}}{1 - m\left(\frac{S_n}{S_u}\right)} \quad \text{for} \quad S_n \leq \sigma_{ys} \tag{2}$$

where K_F and m are the two material parameters. The stress S_u (the ultimate value of elastic nominal stress) was computed from the load required to produce a fully plastic region or hinge [11] on the net section (based on the ultimate tensile strength, σ_u). For the center-crack tension specimen S_u is equal to σ_u. For the three-point notch-bend specimen S_u is $1.5\ \sigma_u$. For the compact specimen S_u is a function of load eccentricity, and is $1.62\ \sigma_u$ for a c/W ratio of 0.5. (See Appendix A.)

The fracture parameters K_F and m are assumed to be constant in the same sense as the ultimate tensile strength; that is, the parameters may vary with material thickness, state of stress, temperature, and rate of loading. To obtain fracture constants that are representative for a given material and test temperature, the nominal failure stress must be less than σ_{ys}, the fracture data should be from a single batch of material of the same thickness, and from tests that encompass a wide range of specimen width or crack length.

If m is equal to zero in Equation (2) K_F is equal to the elastic stress-intensity factor at failure, and the equation represents behavior of low-toughness materials (plane-strain fracture). If m is equal to unity the equation represents behavior of high-toughness materials (plane-stress fracture) [4, 5]. Thus, the fracture-toughness parameters, K_F and m, describe the crack sensitivity of the material.

The denominator in Equation (2) reflects the influence of the nominal failure stress on fracture toughness. The variation of the denominator with nominal stress for a typical material is shown in Figure 2. When the nominal stress is less than the uniaxial yield stress, σ_{ys}, the function ϕ (ratio of K_{Ie} to K_F) is a linear function of nominal stress (solid line). The line has a negative slope, m. However, when the nominal failure stress is greater than the yield stress, the function ϕ becomes nonlinear and is dependent upon the stress-strain curve of the material and the state of stress in the crack-tip region, as discussed in [4]. For thin materials, where the state of stress in the crack-tip region is biaxial, the expected behavior is estimated by the dash-dot curve. An equation was chosen to give a simple approximation to the dash-dot curve and is given by

$$\phi = \frac{K_{Ie}}{K_F} = \frac{\sigma_{ys}}{S_n}\left(1 - m\frac{S_n}{S_u}\right) \tag{3}$$

for $\sigma_{ys} < S_n < S_u$ and is shown by the dashed curve. The vertical dashed line truncates the nominal stress at S_u. For thick materials, where the state of stress in the crack-tip region is triaxial, the fracture behavior for $S_n > \sigma_{ys}$ is expected to lie closer to the solid line. The solid vertical line truncates the nominal stress at S_u. The function ϕ, described by the solid lines, was used in [4, 5]. In order to show the expected range of behavior for thickness, both the solid and dashed curves were used for $S_n > \sigma_{ys}$ in the section on "Analysis of Test Data."

FAILURE PREDICTIONS

After the fracture toughness parameters K_F and m have been determined from fracture tests on a given material and test temperature, Equations (2) and (3) can be used to predict failure stresses for other cracked configurations. The failure stresses were calculated by substituting Equation (1) into Equations (2) and (3), and were given by

$$S_n = \frac{K_F}{\sqrt{\pi c}\ F + \frac{m\ K_F}{S_u}} \quad \text{for} \quad S_n \leq \sigma_{ys} \tag{4}$$

and

$$S_n = \sqrt{(m\gamma)^2 + 2\gamma S_u} - m\gamma \quad \text{for} \quad S_u > S_n > \sigma_{ys} \tag{5}$$

where

$$\gamma = \frac{K_F\ \sigma_{ys}}{2S_u\sqrt{\pi c}\ F} \tag{6}$$

Figure 3 shows the computed nominal failure stresses from Equations (4) and (5) normalized to S_u for a typical material as a function of crack length

in an infinite plate subjected to tensile loading. The tensile and fracture properties for this material are given in Figure 3. The solid curve shows the calculations from Equation (4) for nominal failure stresses less than and greater than the yield stress of the material. For small crack lengths (less than about 1 mm for this material), Equation (4) predicts nominal failure stresses greater than S_u, but in these cases S_n was set equal to S_u. The dash-dot curve in Figure 3, which shows the expected behavior for a thin material ($S_n > \sigma_{ys}$), was calculated by using the function ϕ, described by the dash-dot curve in Figure 2. The dashed curve shows the calculations from Equation (5) for $S_n > \sigma_{ys}$. For stress levels greater than the yield stress, Equation (4) (solid curve) predicts failure stresses higher than expected for thin center-crack tension, compact, and notch-bend specimens made of ductile materials, but closely approximates the failure stresses for surface-cracked specimens [4]. Because the function ϕ, given by Equation (3), is a simple approximation to the expected behavior, Equations (3) and (5) should be used only to estimate failure stresses for $S_n > \sigma_{ys}$ and not to obtain K_F and m from nominal failure stresses in that range.

ANALYSIS OF TEST DATA

Fracture data from the literature on center-crack tension, compact, and notch-bend specimens made of steel, titanium, or aluminum alloy sheet and plate material were analyzed using the two-parameter fracture criterion. The fracture constants, K_F and m, were determined from the fracture data using Equation (2) and a best-fit procedure [4]. In some cases, to illustrate that K_F and m are material parameters, they were determined from one type of specimen and were then used to predict the failure stresses for other types of specimens. In the following sections all of the fracture data are presented

in terms of the elastic stress-intensity factor at failure, K_{Ie}. The experimental K_{Ie} values are compared with either calculated or predicted values as a function of crack length or specimen width. The calculated or predicted K_{Ie} values were obtained by substituting the failure stresses computed from Equations (4) or (5) into Equation (1) and were given by

$$K_{Ie} = \frac{K_F}{1 + \frac{m K_F}{S_u \sqrt{\pi c}\, F}} \quad \text{for} \quad S_n \leq \sigma_{ys} \tag{7}$$

$$K_{Ie} = \left\{ \sqrt{(m\gamma)^2 + 2\gamma S_u} - m\gamma \right\} \sqrt{\pi c}\, F \quad \text{for} \quad S_u > S_n > \sigma_{ys} \tag{8}$$

and

$$K_{Ie} = S_u \sqrt{\pi c}\, F \quad \text{for} \quad S_n = S_u \tag{9}$$

The "calculated" K_{Ie} values were obtained by a best fit of Equation (7) or (8) to the experimental data. The "predicted" values were obtained from Equation (7) or (8) where K_F and m were determined from fracture tests conducted on a different specimen type. Equation (7) was also used for $S_n > \sigma_{ys}$ in order to show the expected range of behavior for thickness as discussed previously.

Aluminum Alloy Specimens

Tests on 7075-T6 and 2024-T3—Fracture tests were conducted on center-crack tension specimens (Fig. 1(a)) made of 7075-T6 or 2024-T3 material (NASA Langley data, Table I) to demonstrate that the fracture criterion applies over a wide range of material fracture toughness. The fracture data (square symbols for 7075-T6 and circular for 2024-T3) are shown in Figure 4 as K_{Ie} plotted against crack-length-to-width ratio. The solid symbols denote tests for which S_n was greater than σ_{ys}. The K_{Ie} values for the 7075-T6 were nearly

constant, as expected, for a low-toughness material (K_F = 31 MN/m$^{3/2}$). In contrast to the low-toughness behavior of the 7075-T6, the 2024-T3 sheet material exhibited a high-fracture toughness (K_F = 267 MN/m$^{3/2}$). Because the failure stresses for the 2024-T3 specimens were nearly equal to the yield stress of the material, K_{Ie} varied significantly with crack length. The solid curves show the calculated results from the fracture criterion (Eq. (7)) using the values of K_F and m determined from a best fit of these data. The dashed curves (at crack-length-to-width ratios less than 0.15 and greater than 0.85 for the 2024-T3 alloy) show the calculated behavior for $S_n > \sigma_{ys}$ using Equation (8). The calculations from Equation (7) for $S_n > \sigma_{ys}$ (not shown) nearly overlapped the dashed curve. For both materials, the calculated results were in good agreement with the experimental results.

Tests on 2219-T851—Kaufman and Nelson [12] conducted fracture tests on compact specimens (Fig. 1(b)) made of 2219-T851 plate material for various specimen thicknesses, widths, and crack lengths. The plate thickness analyzed was 25.4 mm and the c/W ratio was 0.5. Figure 5 shows the experimental (symbols) and calculated (curves) K_{Ie} values plotted against specimen width. The fracture constants, K_F and m, were determined from these data ($S_n < \sigma_{ys}$). The solid symbols denote fracture tests for which S_n was greater than σ_{ys}. The solid and dashed curves were calculated using Equations (7) and (8), respectively. Equation (7) was applied over the complete range of specimen widths, even though S_n was greater than σ_{ys}, to show that the two equations give about the same results (within 10 percent) for $W < 100$ mm. For wide specimens, the calculated K_{Ie} values approach the fracture toughness K_F (indicated by the dash-dot line).

The results of fracture tests conducted on 38-mm-thick compact specimens [12] at various c/W ratios for a constant specimen width (150 mm) are shown in Figure 6(a). The fracture constants K_F = 65.8 MN/m$^{3/2}$ and m = 0.89 were obtained from data (not shown) on the same material and thickness where the c/W ratio was held constant at 0.5 and the specimen width was varied between 75 and 150 mm. Since these fracture properties were obtained from tests with a constant c/W, they do not inherently account for variations in K_{Ie} with c/W. The curve in Figure 6(a) shows the predictions using Equation (7). The agreement between the experimental and predicted results is considered good. Figure 6(b) shows how the pin-loaded holes in the compact specimen influences nominal failure stresses. The symbols show the experimental failure stresses plotted against c/W for the same data shown in Figure 6(a). The solid and dashed curves show the predictions using Equation (4) and the boundary-correction factors obtained with [13] and without (ASTM E399-74) the pin-loaded holes. The good agreement between the experimental and predicted results (solid curve) at the small c/W ratios can be attributed to including the influence of the pin-loaded holes on stress intensity.

Tests on Hiduminium-48—Adams and Munro [14] conducted fracture tests on center-crack tension specimens made of Hiduminium-48, an aluminum alloy sheet material, over a wide range of crack lengths and specimen widths. The material thickness for all specimens was 3.2 mm. The experimental results (symbols) are presented in Figure 7(a) as K_{Ie} plotted against 2c/W for specimen widths ranging from 50 to 200 mm. The curves were calculated using Equation (7) or (8) depending on nominal stress levels, with K_F = 405 MN/m$^{3/2}$ and m = 0.95 (best fit to these data). The two-parameter fracture criterion correlated the data within ±4 percent for all crack lengths and specimen widths. (The solid

curves for $S_n > \sigma_{ys}$ nearly overlapped the dashed curves and were not shown to simplify the plot.)

Adams and Munro [14] also conducted fracture tests on compact specimens made of the same Hiduminium-48 sheet material previously described. The compact specimen fracture data were analyzed using the fracture constants, K_F and m, determined from the center-crack tension specimens. Figure 7(b) shows the experimental (symbols) and predicted (dashed curve) K_{Ie} values plotted against specimen width. The predicted K_{Ie} values fell within ± 10 percent of the experimental results, even though the nominal failure stresses were 20 to 50 percent higher than the yield stress of the material. The solid curve, predicted from Equation (7), is about 15 percent higher than the experimental K_{Ie} values. These predictions also indicate that specimen widths much larger than 250 mm would be required to obtain failures with $S_n < \sigma_{ys}$.

Tests on 7075-T6 Clad and 2014-T3—Bradshaw and Wheeler [15] conducted fracture tests on center-crack tension and compact specimens made of four different aluminum alloy sheet materials. All specimens were 1.6 mm thick. Only the analysis of the materials with the highest and lowest yield stress (7075-T6 clad and 2014-T3, respectively) are shown.

The fracture constants, K_F and m, for the two aluminum alloys were determined from an analysis of the center-crack specimen data (not shown). The center-crack specimens were either 250 or 750 mm wide and the crack-length-to-width ratio ranged from 0.1 to 0.5. The fracture properties $K_F = 77.6$ MN/m$^{3/2}$ and $m = 0.43$ were obtained from the 7075-T6 data and $K_F = 273$ MN/m$^{3/2}$ and $m = 1$ from the 2014-T3 data.

The fracture properties determined from the center-crack tension specimens were then used to predict the failure of the compact specimens. The elastic

stress-intensity factor for the compact specimens used in [15], which were not standard ASTM (E399-74) specimens, was

$$K_I = \frac{P}{t\sqrt{W}} 3.7 \quad \text{for} \quad \frac{c}{W} = 0.17 \tag{10}$$

Figure 8 shows the experimental K_{Ie} values (symbols) plotted against specimen width for the 7075-T6 clad material. The solid and dashed curves show the predicted K_{Ie} values using Equations (7) and (8), respectively. The predicted behavior was within ± 7 percent of the experimental results.

Figure 9 shows the experimental (symbols) and predicted (dashed curve) K_{Ie} values plotted against specimen width for the 2014-T3 compact specimens. The nominal failure stresses for all of the specimens were greater than σ_{ys}. The dashed curve shows the predicted behavior using Equation (8) with the values of K_F and m that were determined from the center-crack specimen fracture data. The predicted behavior was within ± 5 percent of the experimental results. Again, the solid curve shows how Equation (7) overpredicts the experimental failure stresses for thin materials when the nominal failure stresses are greater than σ_{ys}.

Ti-6Al-4V Titanium Alloy Specimens

Gunderson (Air Force Materials Laboratory, AFML-MXE 73-3) conducted fracture tests on compact specimens made of a beta-processed mill-annealed plate of Ti-6Al-4V (25.4 mm thick). Figure 10 shows the experimental (symbols) and calculated (curves) K_{Ie} values plotted against specimen width. The c/W ratio for these data was 0.5. The values of K_F and m used in the calculations were determined from an analysis of these data. The calculated results (solid and dashed curves) for $c/W = 0.5$ agreed well with the experimental results. The curves for $c/W = 0.2$ and 0.8 show how K_{Ie} varies as a

function of c/W. These results indicate that for larger c/W ratios wider specimens are required to obtain $S_n < \sigma_{ys}$ (intersection of solid and dashed curves denote where $S_n = \sigma_{ys}$). All three curves approach the fracture toughness, K_F (dash-dot line), for very wide specimens.

4340 Steel Specimens

Jones and Brown [16] conducted fracture tests on three-point notch-bend specimens (Fig. 1(c)) made of 4340 steel with several strength levels. These tests were conducted to determine the influence of thickness, crack length, and specimen width on fracture toughness. Figure 11 shows the results of fracture tests (symbols) conducted on 1.3 and 25.4 mm thick specimens with c/W = 0.5 for various specimen widths. The curves were calculated using either Equation (7) or (8) with K_F and m determined by a best fit for each material thickness. For the thin material, all of the test data had nominal failure stresses greater than the yield stress of the material. Therefore, the values of K_F and m were determined using Equation (8). (The values of K_F and m should have been obtained from testing specimens with widths greater than 75 mm where the nominal failure stresses would have been less than σ_{ys}, but no fracture data were available with widths greater than 75 mm.) For the thicker material, K_F was equal to K_{Ic}, the plane-strain fracture toughness, and K_{Ie} values were independent of specimen width.

PLANE-STRESS AND PLANE-STRAIN FRACTURE

The two-parameter fracture criterion derived in References [4] and [5] gave a linear relationship between K_{Ie} and the nominal failure stress, S_n, for $S_n < \sigma_{ys}$. The three-dimensional diagram in Figure 12 shows how the experimental values of K_{Ie} (square symbols) vary as a function of nominal failure stress (normalized to S_u) and plate thickness for compact specimens made of

2219-T851 aluminum alloy [12]. The experimental relationship between K_{Ie} and S_n is, also, approximately linear. The three-dimensional surface, formed by the straight-line generators (solid lines), is the locus of K_{Ie} values for various combinations of specimen dimensions. The ASTM standard test procedure (E399-74) is intended to produce a constant value of plane-strain fracture toughness, K_{Ic}. Such behavior would produce a plateau near the left extremity of the surface shown (with $m = 0$). For many materials of practical interest the specimens required to produce plane-strain fracture are so large that testing is very difficult, if not impossible. Thus, the two-parameter fracture criterion can be useful for computing fracture toughness and predicting failure stresses for structural materials which fracture under either plane-stress or plane-strain conditions.

CONCLUDING REMARKS

A two-parameter fracture criterion that relates the elastic stress-intensity factor at failure, the elastic nominal failure stress, and two material parameters was used to analyze fracture data on center-crack tension, compact, and notch-bend specimens made of steel, titanium, or aluminum alloy materials tested at room temperature. The specimens had a wide range of crack lengths, specimen widths, specimen thicknesses, and material properties. The fracture criterion correlated the data well (generally within ± 10 percent of the experimental failure stresses) for a broad range of materials, including some regarded as very ductile. The fracture criterion was also found to correlate fracture data from different specimen types (such as center-crack tension and compact specimens), within ± 10 percent for the same material, thickness, and test temperature.

REFERENCES

[1] "Plane Strain Crack Toughness Testing of High Strength Metallic Materials," ASTM STP 410, 1966.

[2] "Fracture Toughness Testing," ASTM STP 381, 1964.

[3] Kuhn, P., "Residual Tensile Strength in the Presence of Through Cracks or Surface Cracks," TN D-5432, National Aeronautics and Space Administration, 1970.

[4] Newman, J. C., Jr., "Fracture Analysis of Surface- and Through-Cracked Sheets and Plates," Engineering Fracture Mechanics Journal, Vol. 5, 1973. (Presented at the Symposium on Fatigue and Fracture, George Washington University, May 1972.)

[5] Newman, J. C., Jr., "Plane Stress Fracture of Compact- and Notch-Bend Specimens," TM X-71926, National Aeronautics and Space Administration, 1973.

[6] Hardrath, H. F., and Ohman, L., "A Study of Elastic and Plastic Stress Concentration Factors Due to Notches and Fillets in Flat Plates," Rep. 1117, National Advisory Committee for Aeronautics, 1953. (Supersedes NACA TN 2566.)

[7] Neuber, H., "Theory of Stress Concentration for Shear-Strained Prismatical Bodies With Arbitrary Non-Linear Stress-Strain Law," Transactions, American Society of Mechanical Engineers, Ser. E, Journal of Applied Mechanics, 28, 544-550, 1961.

[8] Hutchinson, J. W., "Singular Behavior at the End of a Tensile Crack in a Hardening Material, Journal of Mech. Phys. Solids, 16, 13-31, 1968.

[9] Rice, J. R., and Rosengren, G. F., "Plane Strain Deformation Near a Crack Tip in a Power-Law Hardening Material," Journal of Mech Phys. Solids, 16, 1-12, 1968.

[10] Kuhn, P., and Figge, I. E., "Unified Notch-Strength Analysis for Wrought Aluminum Alloys," TN D-1259, National Aeronautics and Space Administration, 1962.

[11] Timoshenko, S., Strength of Materials, Advanced Theory and Problems, D. Van Nostrand Co., New York, 1956.

[12] Kaufman, J. G., and Nelson, F. G., "More Specimen Size Effects in Fracture Toughness Testing," ASTM STP 559, 1974.

[13] Newman, J. C., Jr., "Stress Analysis of the Compact Specimen Including the Effects of Pin Loading," ASTM STP 560, 1974.

[14] Adams, N. J. I., and Munro, H. G., "A Single Test Method for Evaluation of the J-Integral as a Fracture Parameter," Engineering Fracture Mechanics, Vol. 6, No. 1, Mar. 1974.

[15] Bradshaw, F. J., and Wheeler, C., "The Crack Resistance of Some Aluminum Alloys and the Prediction of Thin Section Failure," Technical Report 73191, Royal Aircraft Establishment, Mar. 1974.

[16] "Review of Developments in Plane Strain Fracture Toughness Testing," ASTM STP 463, 1969.

[17] Srawley, J. E., and Gross, G., "Stress Intensity Factors for Bend and Compact Specimens," Engineering Fracture Mechanics Journal, Vol. 4, No. 3, Sept. 1972.

APPENDIX A. ELASTIC STRESS-INTENSITY FACTORS AND NOMINAL STRESS DEFINITIONS FOR THE CENTER-CRACK TENSION, COMPACT, AND NOTCH-BEND SPECIMENS

In the application of Equations (2) and (3) to center-crack tension, to compact, and to notch-bend specimens, the stress-intensity factor, the nominal stress, and S_u must be determined as a function of crack length and specimen width. The following sections give these equations.

Center-Crack Tension Specimen

For the center-crack specimen (Fig. 1(a)), the elastic stress-intensity factor is given by Equation (1) where

$$S_n = \frac{S}{1 - \lambda} \tag{A1}$$

and

$$F = (1 - \lambda)\sqrt{\sec\left(\frac{\pi\lambda}{2}\right)} \tag{A2}$$

for $0 \leq \lambda < 1.0$ where λ is the crack-length-to-width ratio. The secant term is the finite-width correction on stress intensity and was obtained from [1].

The ultimate value of elastic nominal stress, S_u, for the center-crack specimen is σ_u.

Notch-Bend Specimen

For the notch-bend specimen (Fig. 1(c)), the elastic stress-intensity factor is given by Equation (1) where

$$S_n = \frac{3PL}{t(W - c)^2} \tag{A3}$$

and

$$F = (1 - \lambda)^2 \frac{f(\lambda)}{\sqrt{\pi}} \tag{A4}$$

The function $f(\lambda)$, obtained from [1], was given by

$$f(\lambda) = A_0 + A_1 \lambda + A_2 \lambda^2 + A_3 \lambda^3 + A_4 \lambda^4 \tag{A5}$$

L/W	A_0	A_1	A_2	A_3	A_4
4	1.93	-3.07	14.53	-25.11	25.80
8	1.96	-2.75	13.66	-23.98	25.22

for $0 \leq \lambda \leq 0.6$. Equation (A5) is within 0.2 percent of the more accurate values [17] for c/W ratios (λ) up to 0.6 and is 3.5 percent lower than the correct value at a c/W ratio of 0.7.

The ultimate value of elastic nominal stress, S_u, for the notch-bend specimens is $1.5\ \sigma_u$. This was computed from the load required to produce a fully plastic hinge on the net section using the ultimate tensile strength.

Compact Specimen

For the compact specimen (Fig. 1(b)), the elastic stress-intensity factor is, again, given by Equation (1) where

$$S_n = \frac{P}{t(W - c)} \left[1 + 3 \left(\frac{1 + \lambda}{1 - \lambda}\right)\right] \tag{A6}$$

and

$$F = \frac{(1 - \lambda)\ f(\lambda)}{\sqrt{\pi\lambda} \left[1 + 3 \left(\frac{1 + \lambda}{1 - \lambda}\right)\right]} \tag{A7}$$

The function $f(\lambda)$, obtained from [13], was given by

$$f(\lambda) = 4.55 - 40.32 \lambda + 414.7 \lambda^2 - 1698 \lambda^3 + 3781 \lambda^4 - 4287 \lambda^5 + 2017 \lambda^6 \tag{A8}$$

for $0.2 \leq \lambda \leq 0.8$. Equation (A8) includes the influence of the pin-loaded holes in the compact specimen.

The ultimate value of elastic nominal stress, S_u, for the compact specimen is a function of load eccentricity and is given by

$$S_u = \left\{ \left[\sqrt{1 + \left(\frac{1 + \lambda}{1 - \lambda} \right)^2} - \left(\frac{1 + \lambda}{1 - \lambda} \right) \right] \left[1 + 3 \left(\frac{1 + \lambda}{1 - \lambda} \right) \right] \right\} \sigma_u \tag{A9}$$

For a range of λ between 0.2 and 0.8,

$$S_u = 1.61 \, \sigma_u \tag{A10}$$

agrees to within 4 percent of that given by Equation (A9).

TABLE I. NOMINAL FAILURE STRESSES FOR CENTER-CRACK TENSION SPECIMENS OF 7075-T6 PLATE AND 2024-T3 SHEET MATERIAL

7075-T6 t = 12.7 mm W = 300 mm σ_u = 600 MN/m^2 σ_{ys} = 496 MN/m^2		2024-T3 t = 2.3 mm W = 300 mm σ_u = 490 MN/m^2 σ_{ys} = 356 MN/m^2	
c, mm	S_n, MN/m^2	c, mm	S_n, MN/m^2
8.5	170.6	6.4	364.4
13.0	142.3	12.7	356.1
13.2	135.7	25.4	344.2
17.3	135.3	50.8	329.4
51.4	111.1	76.2	321.3
73.9	92.3	101.5	321.8
101.3	93.0		

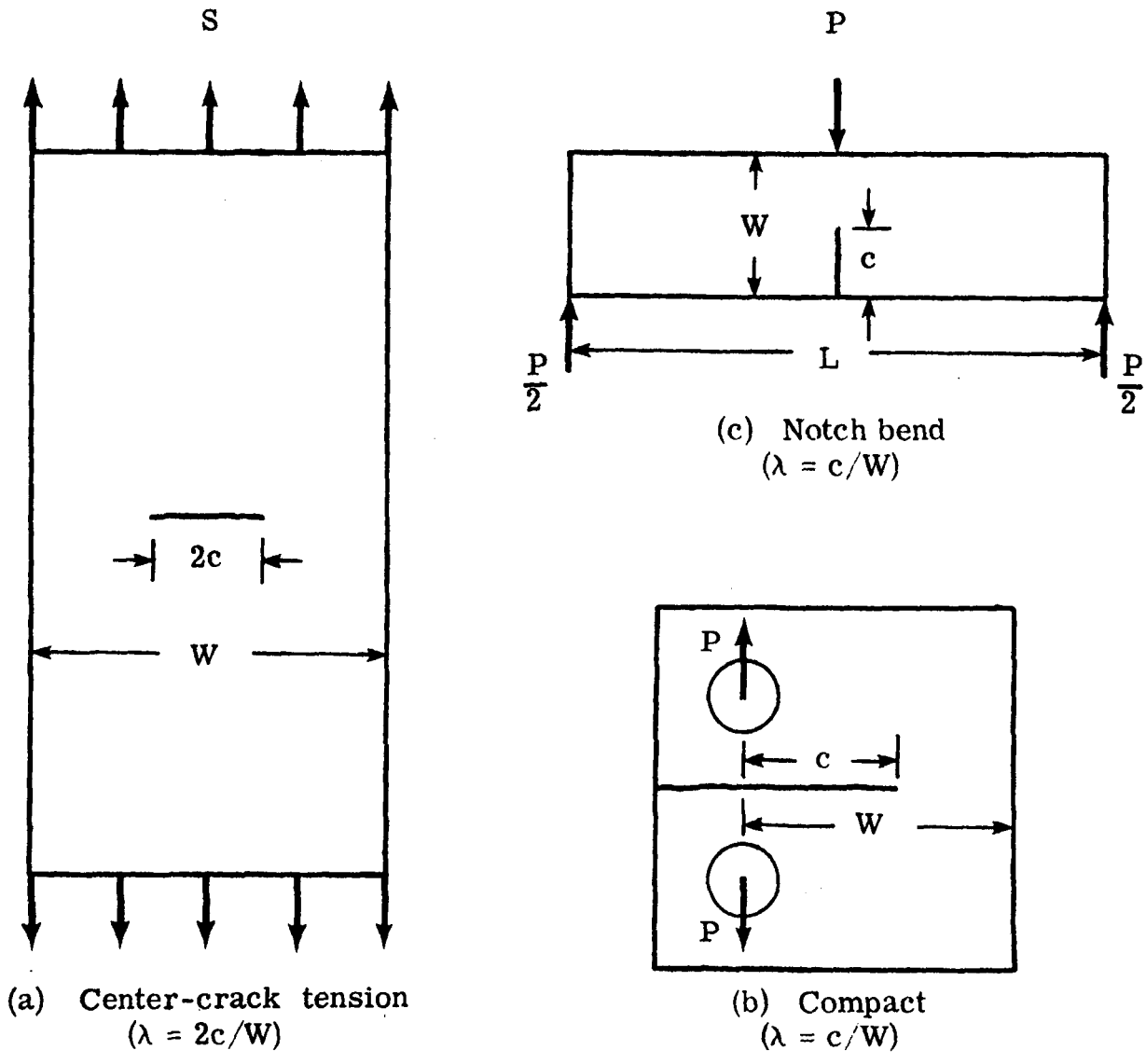

Figure 1. Center-crack tension, compact, and notch-bend specimen configurations.

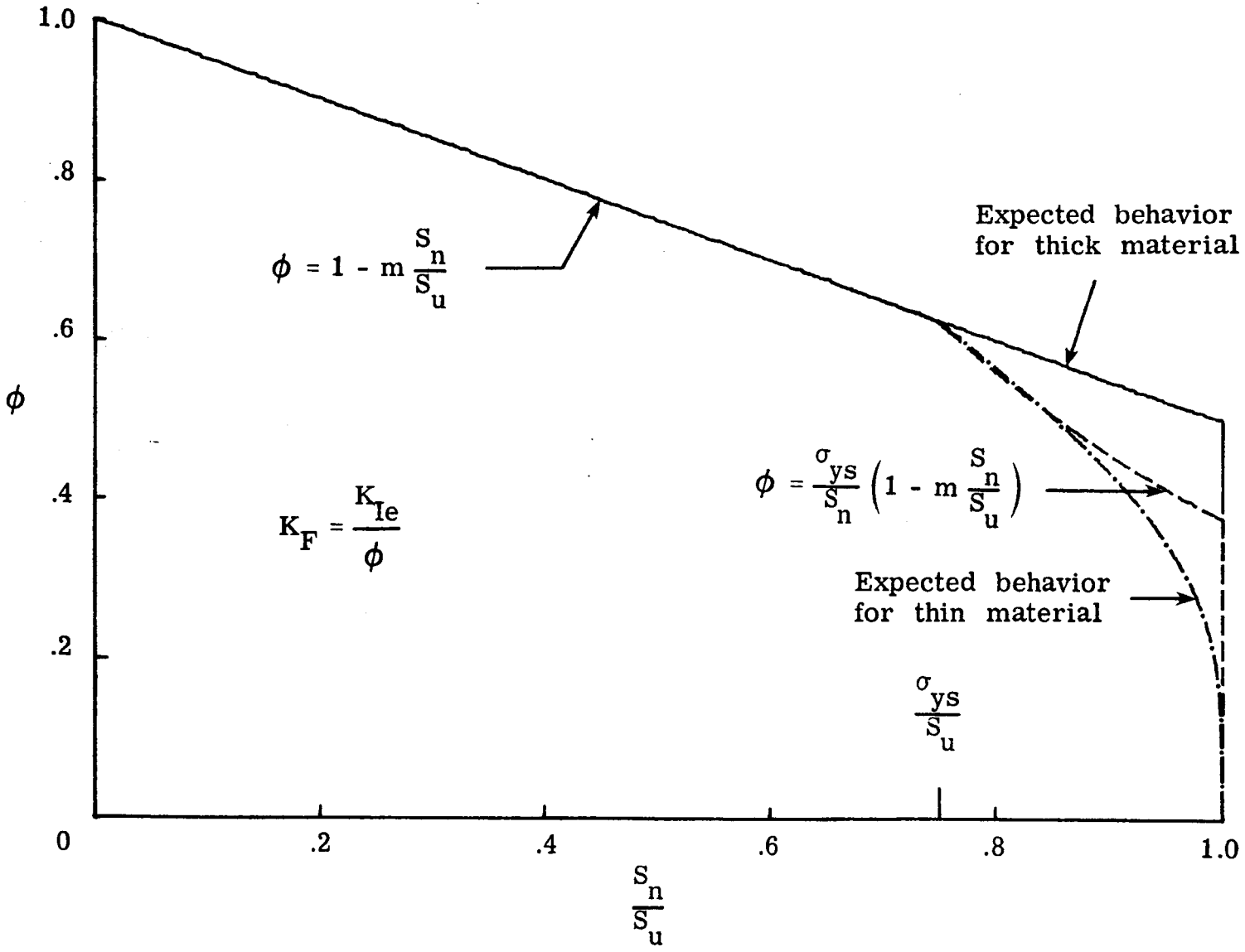

Figure 2. Relationship between ϕ and S_n/S_u.

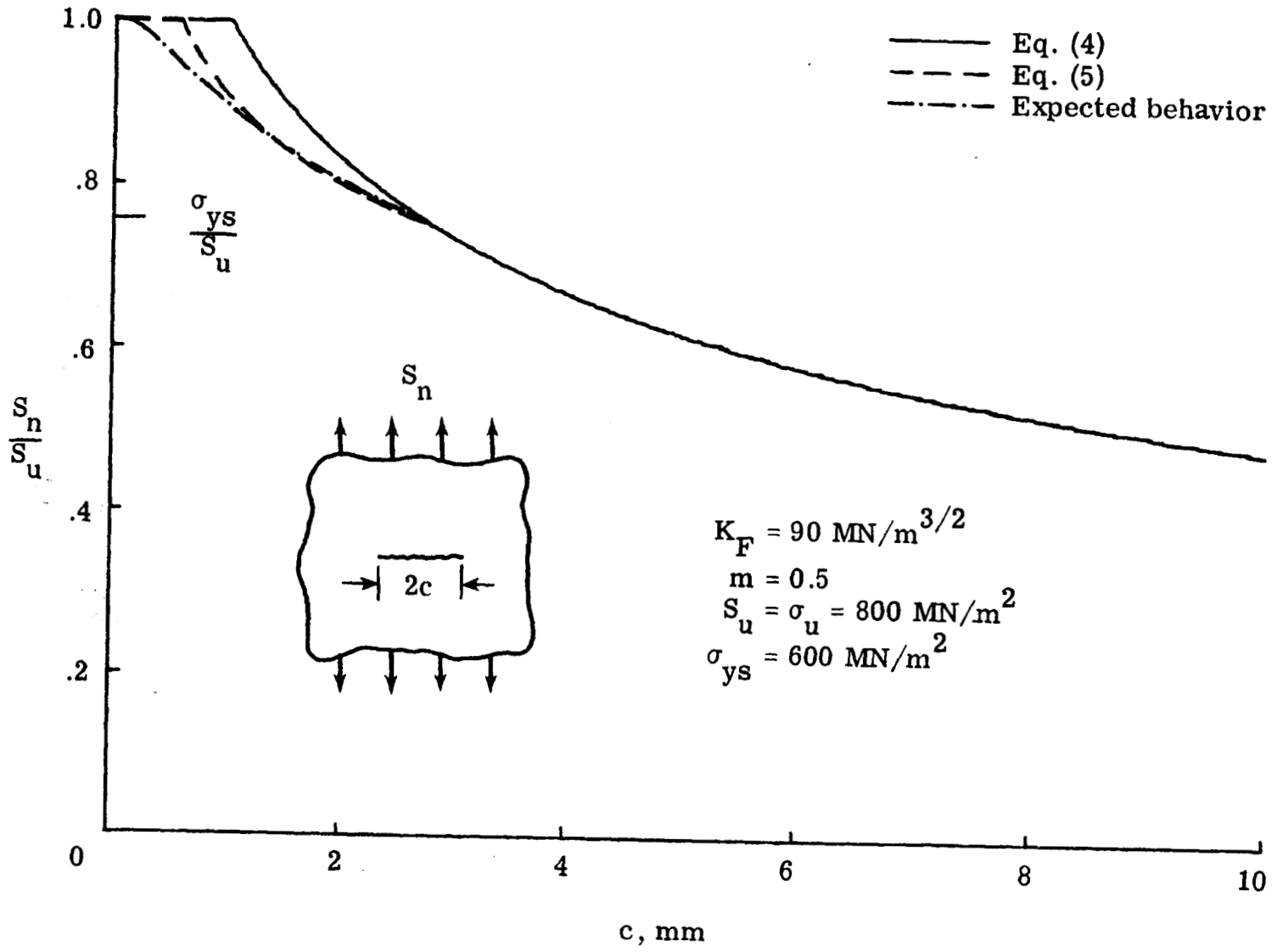

Figure 3. Computed nominal failure stresses as a function of crack length.

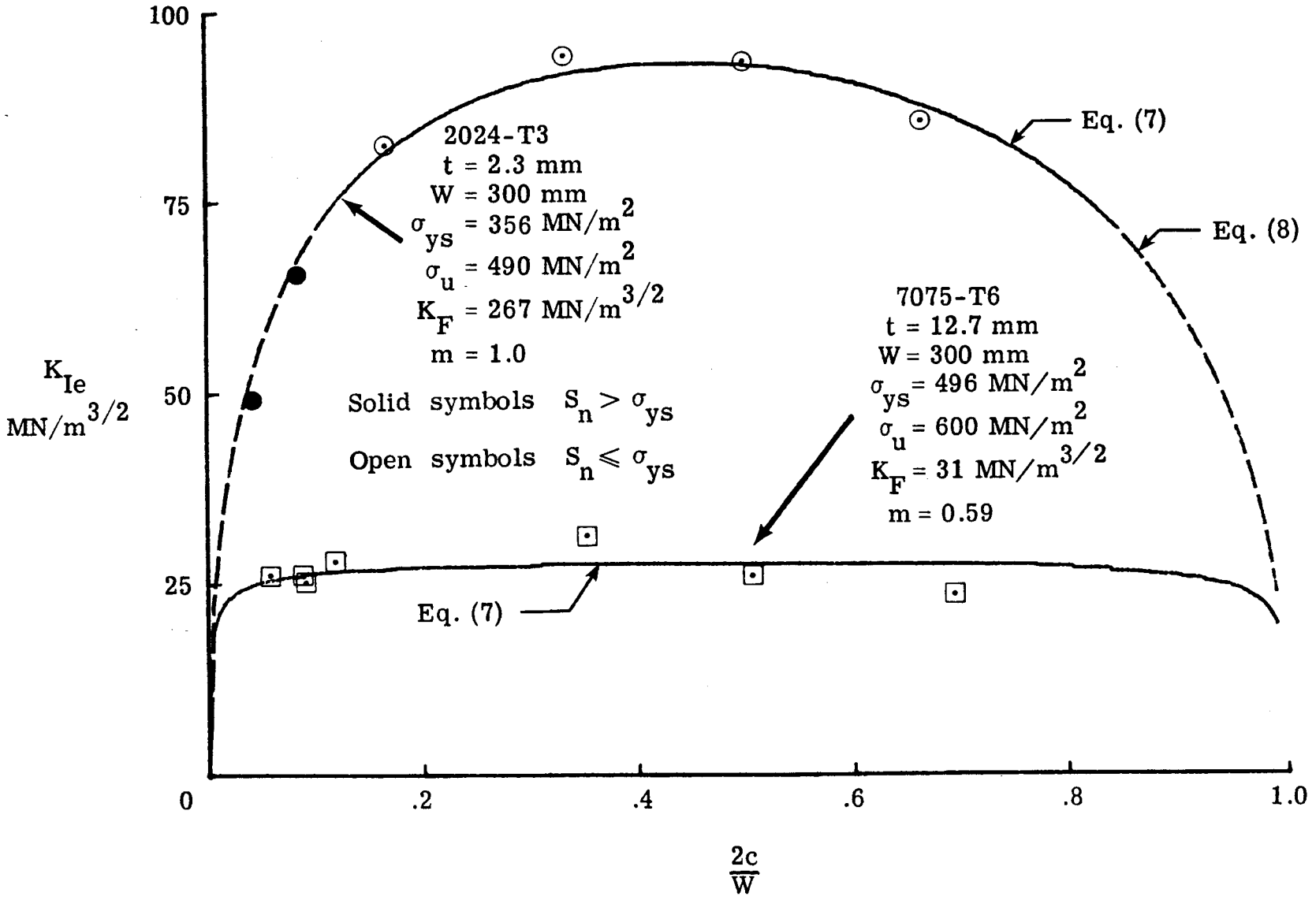

Figure 4. Elastic stress-intensity factors at failure for center-crack tension specimens made of 7075-T6 and 2024-T3 aluminum alloy as a function of crack-length-to-width ratio.

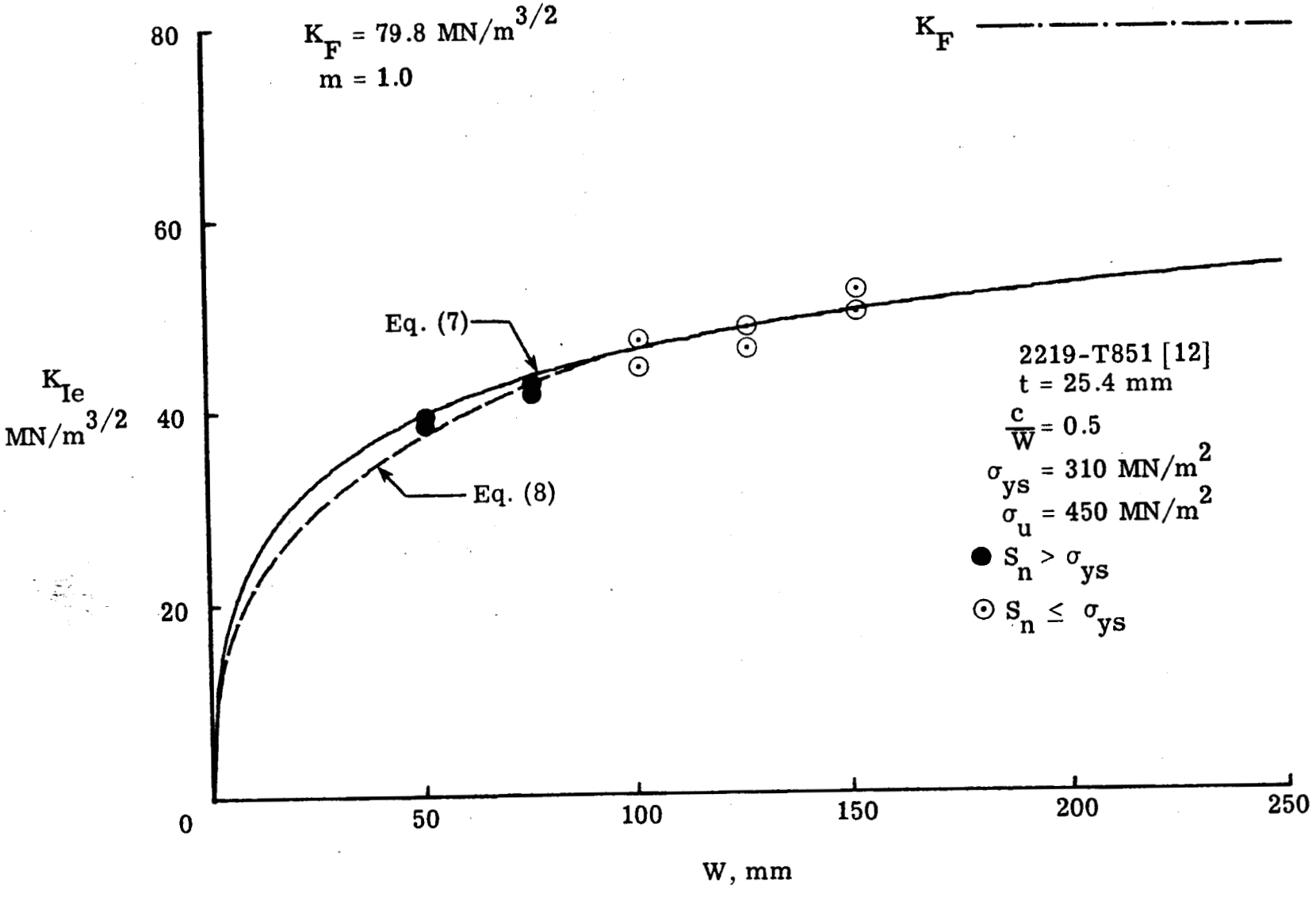

Figure 5. Elastic stress-intensity factors at failure for compact specimens made of 2219-T851 aluminum alloy as a function of specimen width.

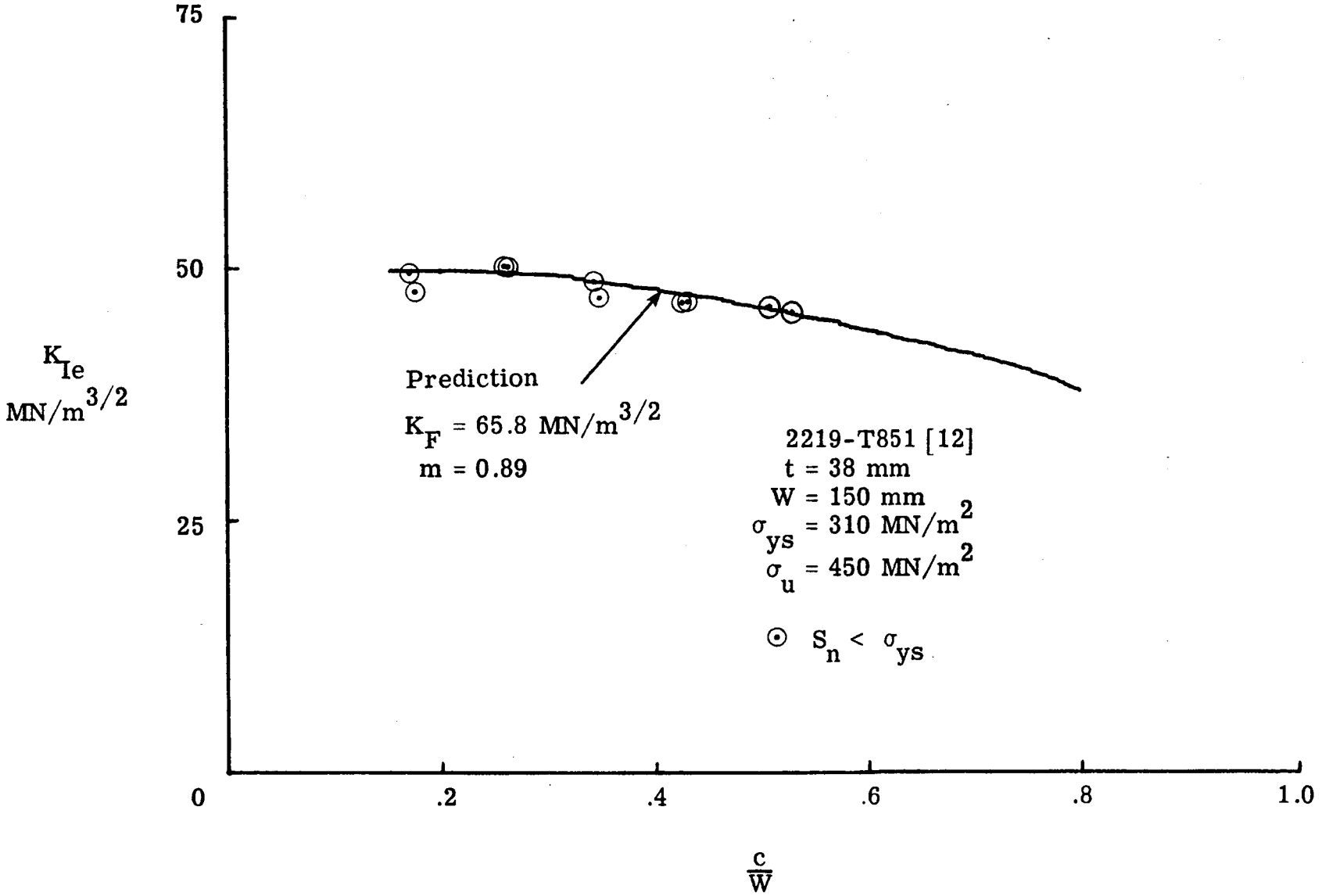

Figure 6(a). Experimental and predicted elastic stress-intensity factors at failure for compact specimens made of 2219-T851 aluminum alloy as a function of crack-length-to-width ratio.

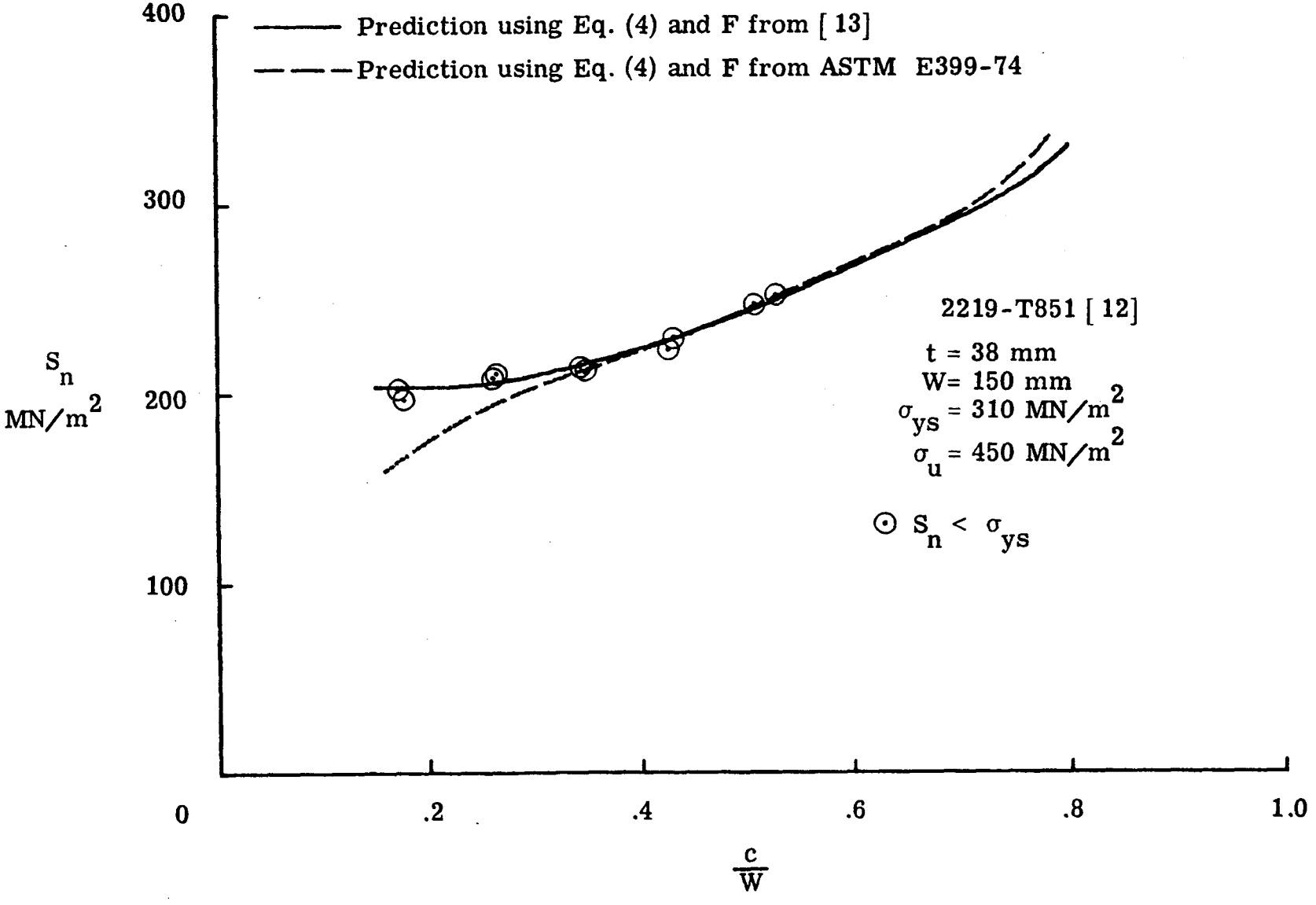

Figure 6(b) Experimental and predicted nominal failure stresses for compact specimens made of 2219-T851 aluminum alloy as a function of crack-length-to-width ratio.

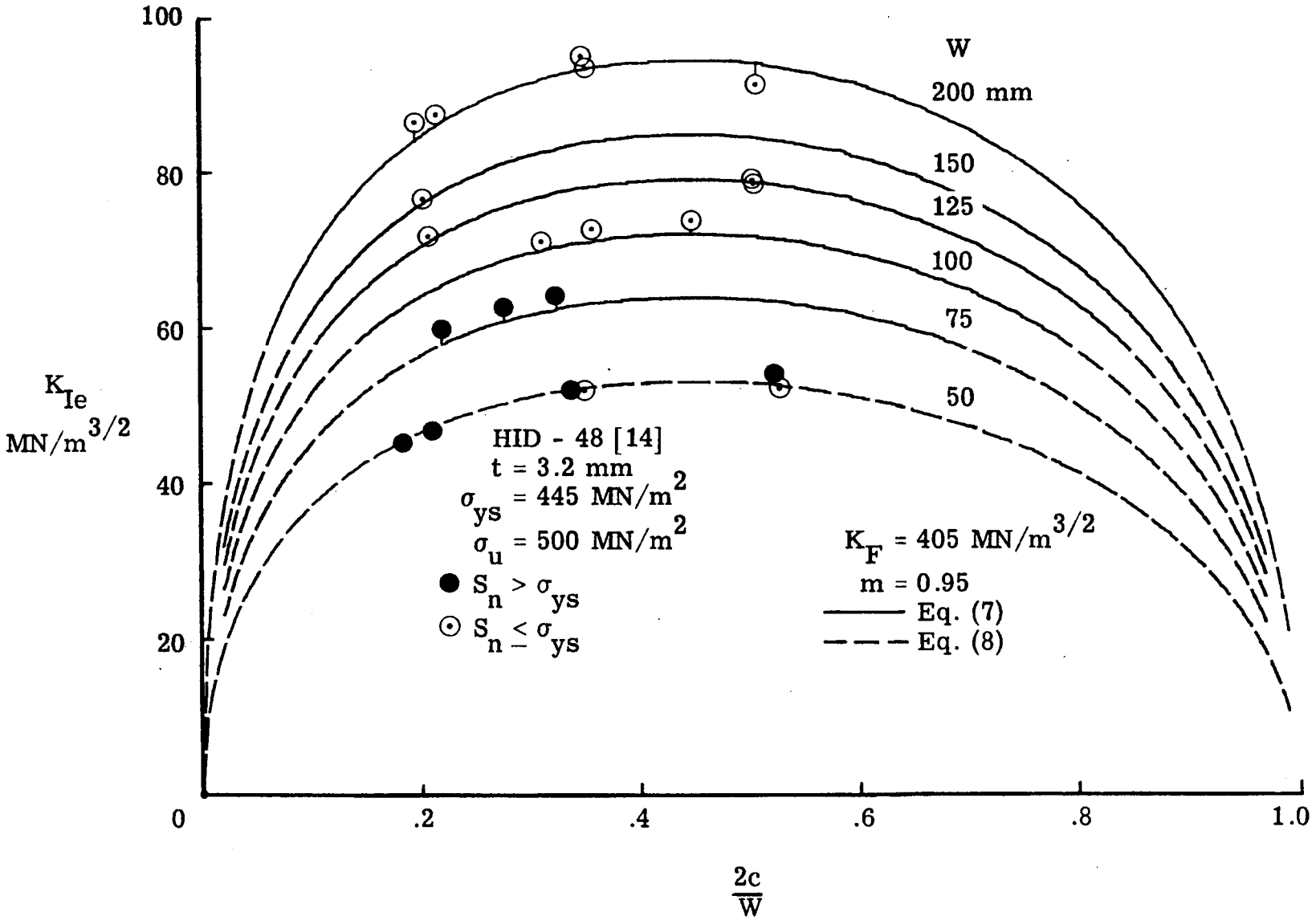

Figure 7(a). Elastic stress-intensity factors at failure for center-crack tension specimens made of Hiduminium-48 sheet material.

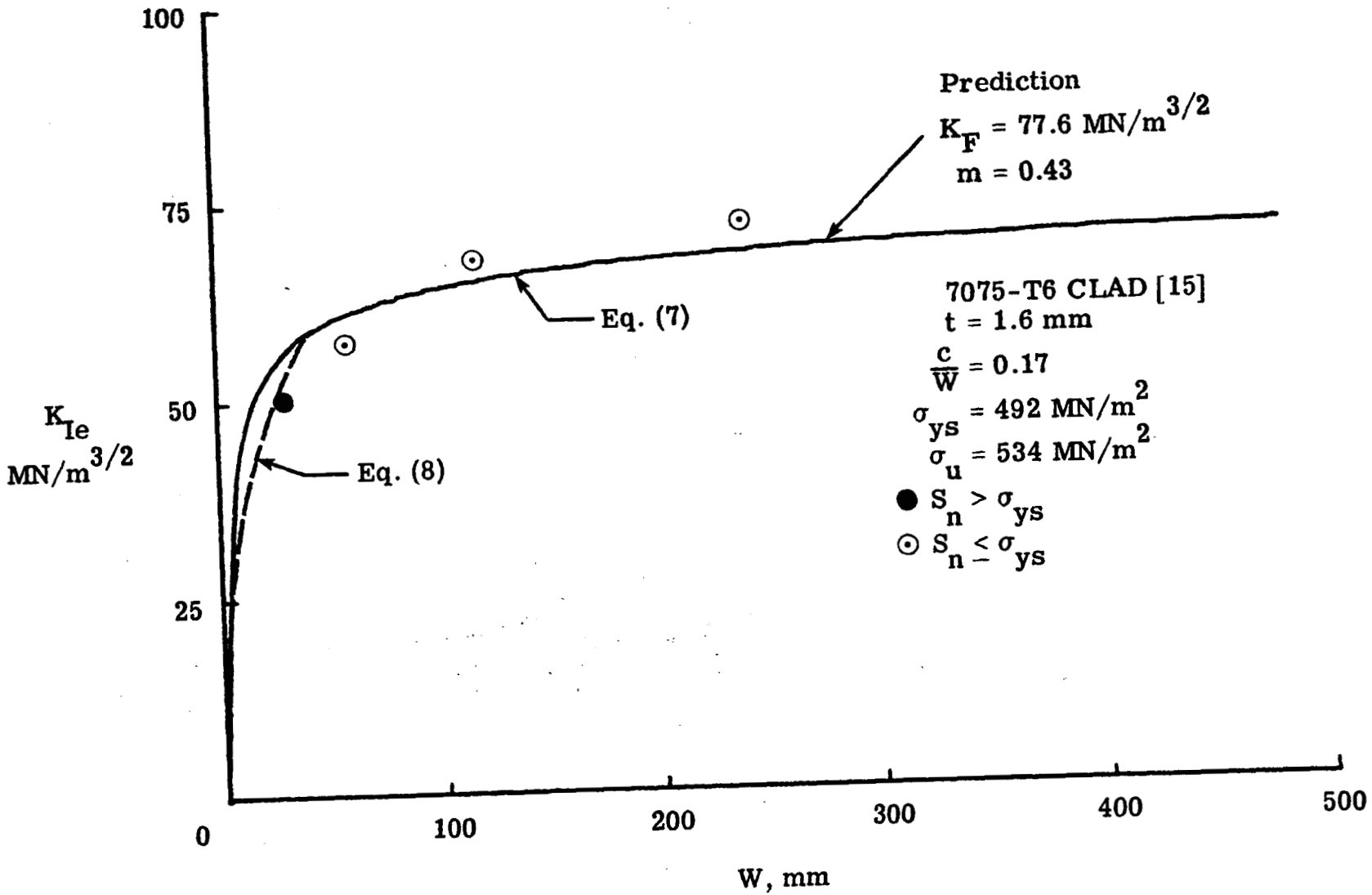

Figure 8. Experimental and predicted elastic stress-intensity factors at failure for compact specimens made of 7075-T6 clad aluminum alloy as a function of specimen width.

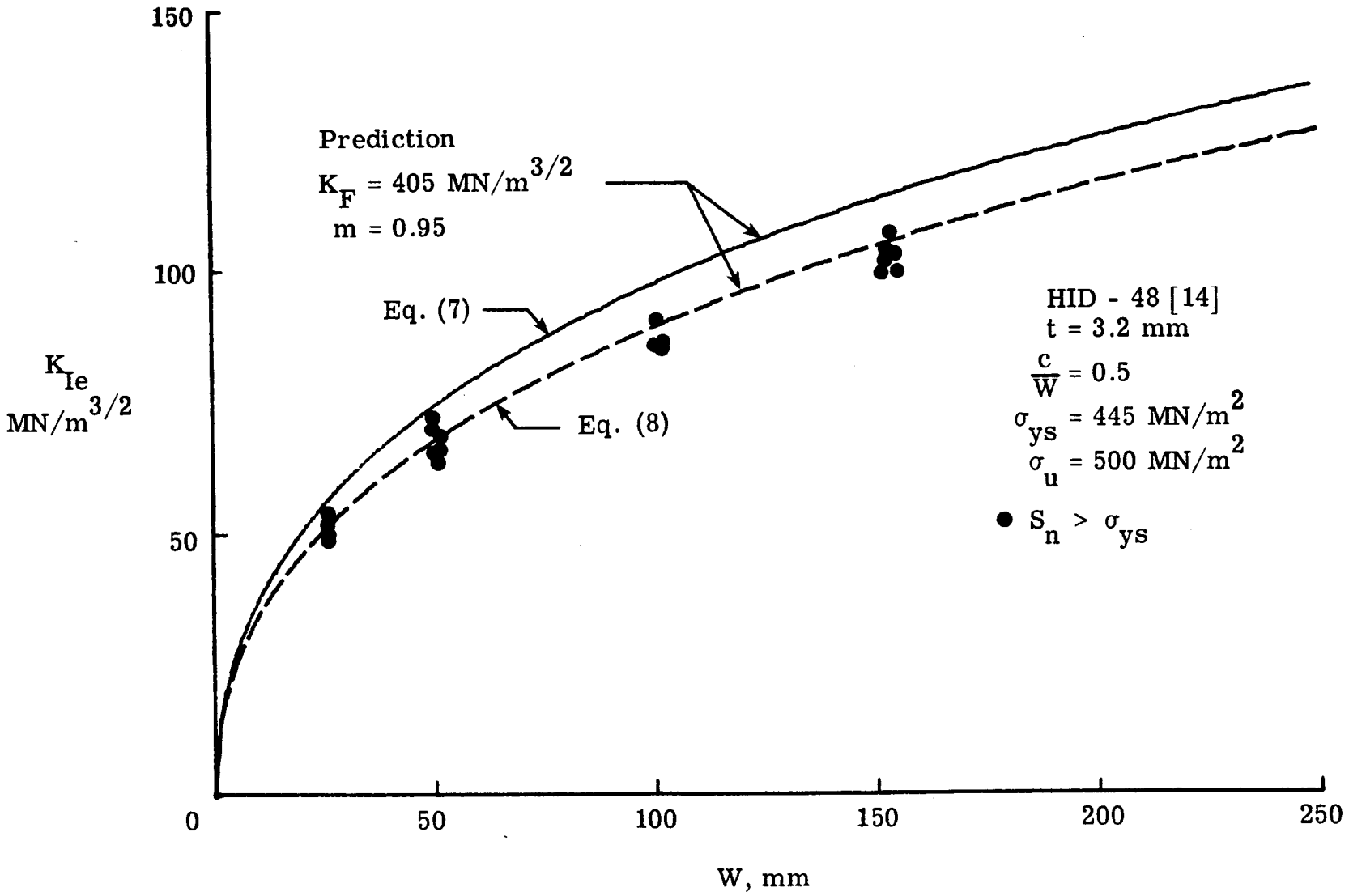

Figure 7(b). Experimental and predicted elastic stress-intensity factors at failure for compact specimens made of Hiduminium-48 sheet material as a function of specimen width.

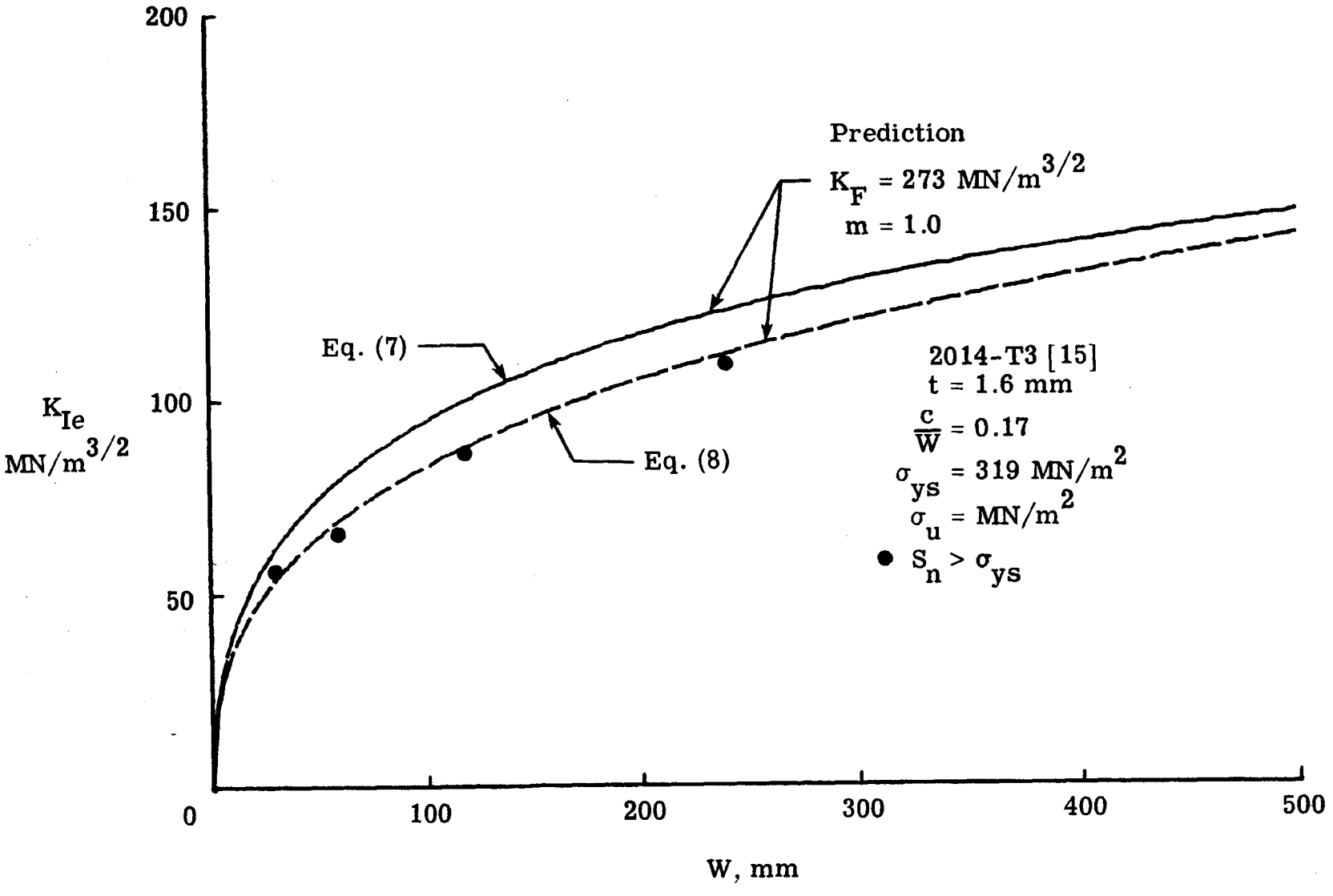

Figure 9. Experimental and predicted elastic stress-intensity factors at failure for compact specimens made of 2014-T3 aluminum alloy as a function of specimen width.

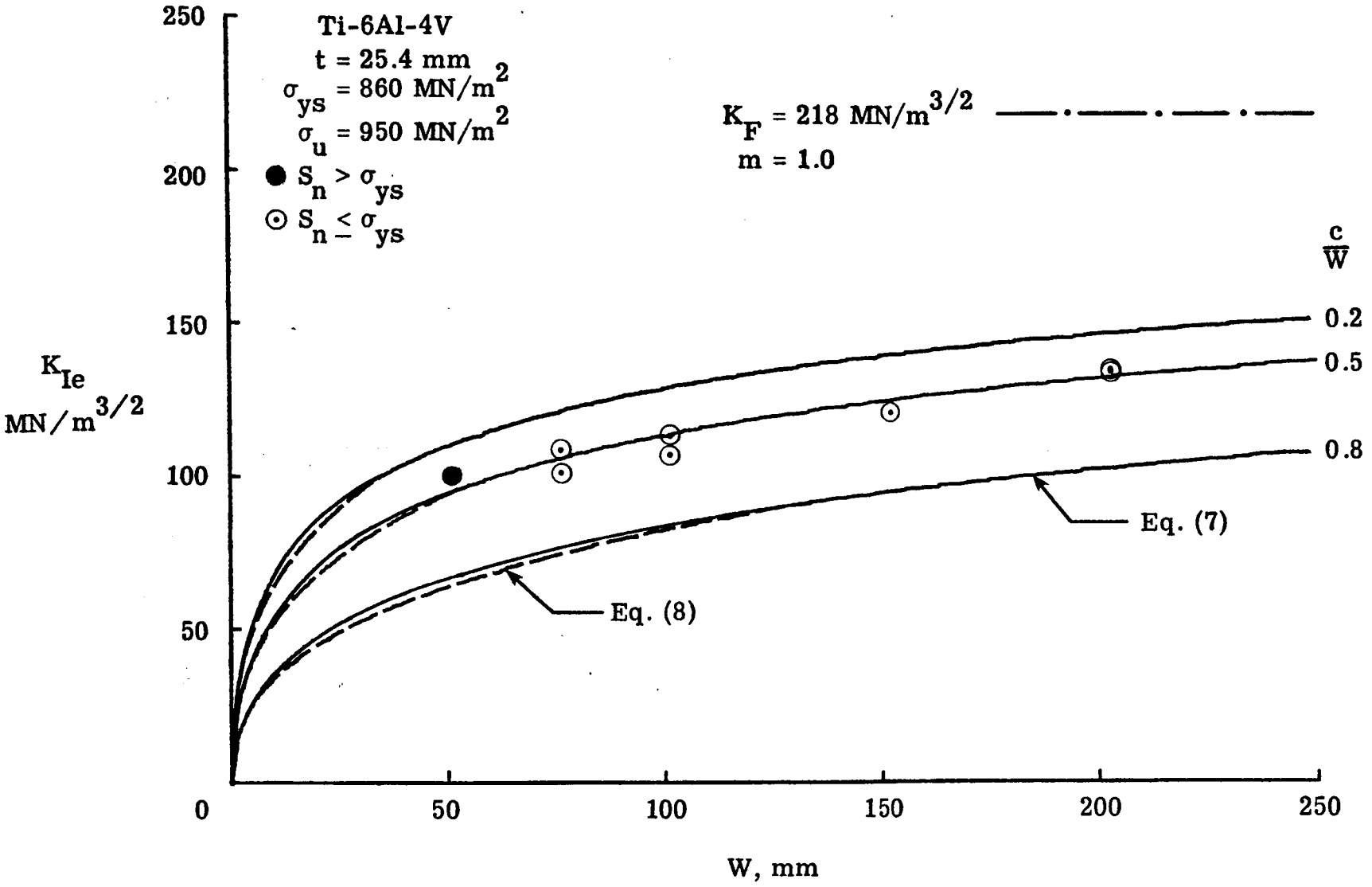

Figure 10. Elastic stress-intensity factors at failure for compact specimens made of Ti-6Al-4V titanium alloy as a function of specimen width.

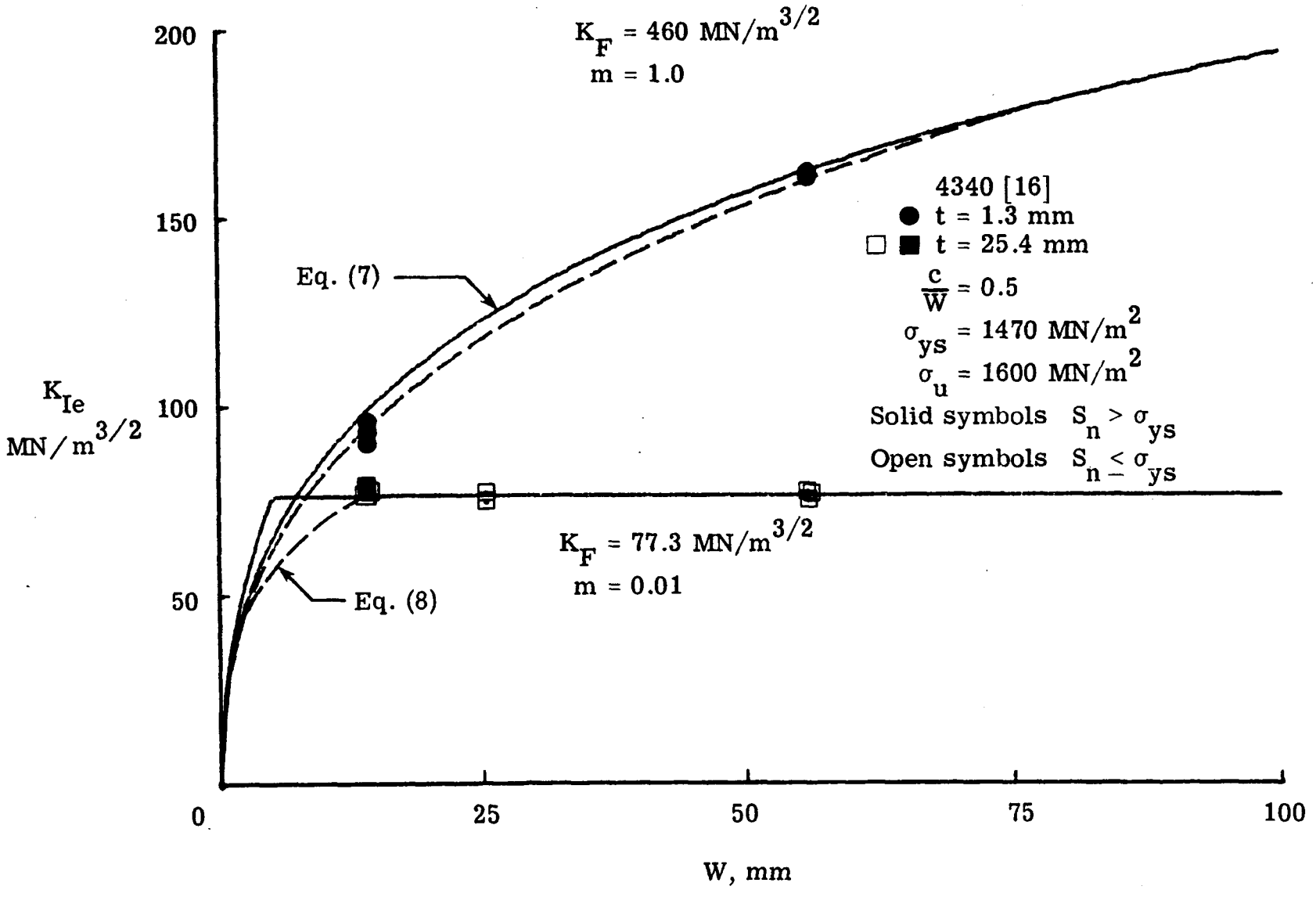

Figure 11. Elastic stress-intensity factors at failure for three-point notch-bend specimens made of 4340 steel (two thicknesses) as a function of specimen width.

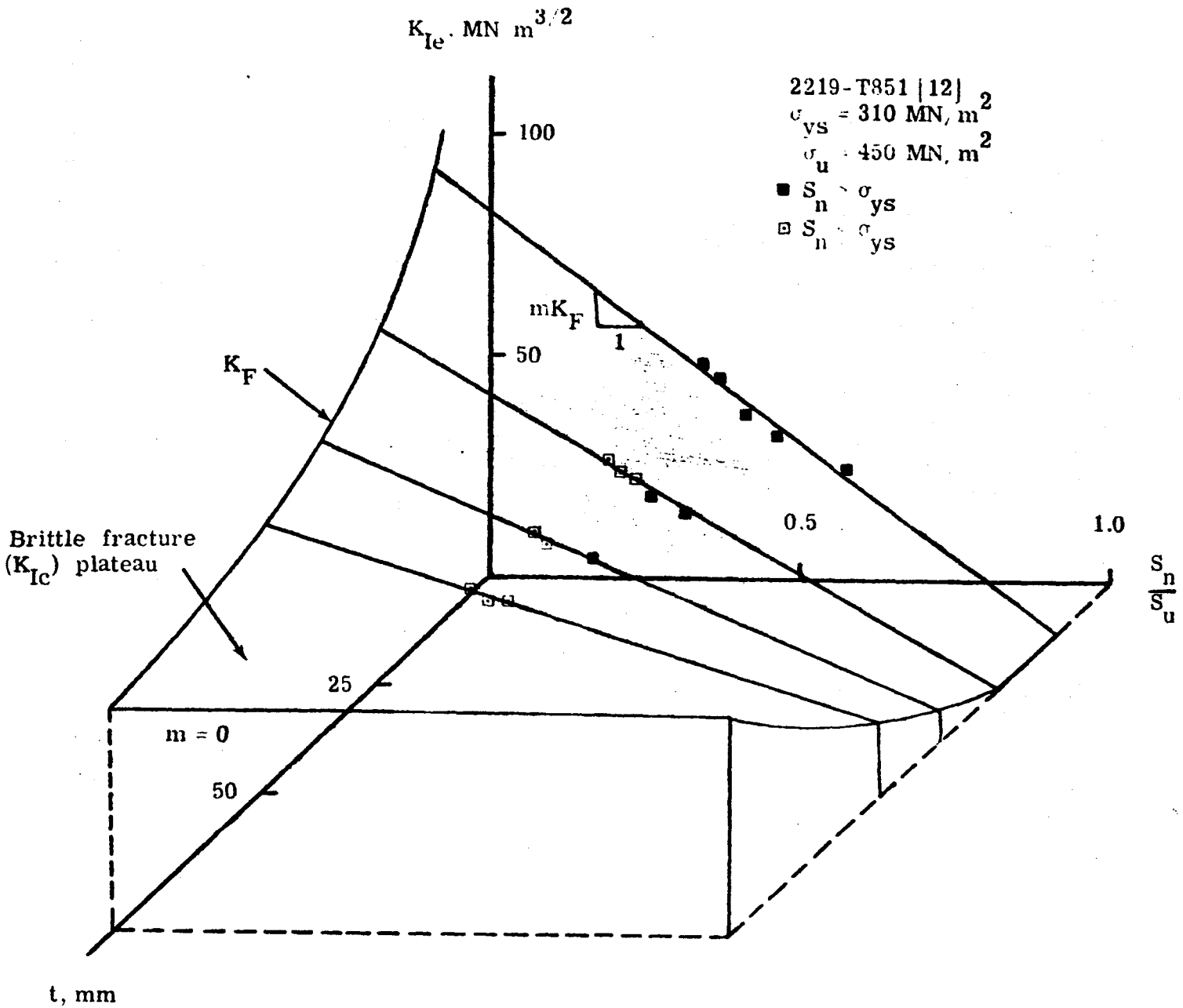

Figure 12. Elastic stress-intensity factors at failure for compact specimens made of 2219-T851 aluminum alloy as a function of nominal failure stress and thickness.